

The integrated radio spectrum of G2.4+1.4

D. A. Green^{*}

Astrophysics Group, Cavendish Laboratory, 19 J. J. Thomson Avenue, Cambridge CB3 0HE

Accepted 2022 August 16. Received 2022 August 15; in original form 2022 May 24

ABSTRACT

The Galactic source G2.4+1.4 is an optical and radio nebula containing an extreme Wolf–Rayet star. At one time this source was regarded as a supernova remnant, because of its apparent non-thermal radio spectrum, although this was based on limited observations. Subsequent observations instead supported a flat, optically thin thermal radio spectrum for G2.4+1.4, and it was identified as a photoionized, mass-loss bubble, not a supernova remnant. Recently, however, it has been claimed that this source has a non-thermal integrated radio spectrum. I discuss the integrated radio flux densities available for G2.4+1.4 from a variety of surveys, and show that it has a flat spectrum at gigahertz frequencies (with a spectral index α of 0.02 ± 0.08 , where flux density S scales with frequency ν as $S \propto \nu^{-\alpha}$).

Key words: ISM: individual objects: G2.4+1.4 – radio continuum: ISM – radiation mechanisms: thermal – radiation mechanisms: non-thermal

1 INTRODUCTION

G2.4+1.4 is an optical and radio source in Sagittarius, ≈ 12 arcmin in extent (e.g. [Treffers & Chu 1982](#); [Green & Downes 1987](#); [Goss & Lozinskaya 1995](#)), showing multiple rings. The Wolf–Rayet star WR 102 is within G2.4+1.4, but is offset from its centre (e.g. [Dopita et al. 1990](#)). It was identified as a supernovae remnant (SNR) based on its non-thermal radio spectrum, as reported by [Johnson \(1975\)](#). Hence it was included in some catalogues of Galactic supernova remnants (e.g. [Milne 1979](#); [Green 1984](#)), although it was removed from subsequent catalogues (i.e. [Green 1988](#)), as the non-thermal radio spectrum was questioned by [Green & Downes \(1987\)](#). [Dopita & Lozinskaya \(1990\)](#) identify G2.4+1.4 as a ‘photoionized, mass-loss bubble’ powered by the WR star. Recently, however, [Prajapati et al. \(2019\)](#) have reported a non-thermal integrated radio spectrum for G2.4+1.4. Here I investigate the radio spectrum of G2.4+1.4 from available radio surveys, and compare this with the results of [Prajapati et al. \(2019\)](#).

Section 2 provides background information on G2.4+1.4 and its radio spectrum. The radio spectrum of G2.4+1.4 based on available survey observations is presented Section 3, and this is discussed in Section 4.

2 BACKGROUND

G2.4+1.4 appeared¹ in various single dish radio observations: i.e. [Goss & Shaver \(1968\)](#) at 5000 MHz, [Beard, Thomas & Day \(1969\)](#) at 2650 MHz, [Altenhoff et al. \(1970\)](#) at 2695 MHz, and [Sinclair & Kerr \(1971\)](#) at 1410 MHz, as listed in [Johnson \(1975\)](#). These single dish observations are of low-resolution (≈ 4 arcmin at best), and do not resolve G2.4+1.4 well, some giving sizes for the source between

5 and 9 arcmin. The flux densities between 1410 and 5000 MHz are between 2 and 5 Jy. [Johnson \(1975\)](#) presented higher frequency observations of G2.4+1.4, at both 15.5 and 31.4 GHz, with much smaller flux densities than the available flux densities at lower frequencies. However, no error was given for the 15.5-GHz flux density, and the 31.4-GHz value was very uncertain (0.34 ± 0.26 Jy, i.e. a nominal detection at less than the 1.5σ level). Because of the lower flux densities at the higher frequencies [Johnson](#) deduced a non-thermal radio spectrum for G2.4+1.4, and identified it as supernova remnant, albeit one that unusually contains an high excitation star. Subsequently [Treffers & Chu \(1982\)](#) reported optical observations of G2.4+1.4, showing a ‘complex double shell structure’. They concluded that G2.4+1.4 is a SNR, and noted that its non-thermal radio emission was the strongest argument for this identification.

The non-thermal radio spectrum, and the SNR identification for G2.4+1.4 was not supported by [Caswell & Haynes \(1987\)](#), who presented 5-GHz radio observations of the source. They derived a flux density of 2.5 Jy for G2.4+1.4 at 5 GHz, with a size of 6×8 arcmin², and detected hydrogen recombination line emission from it. Hence they concluded the radio emission from G2.4+1.4 is thermal. [Green & Downes \(1987\)](#) presented VLA observations of G2.4+1.4 at 4860 MHz with a much higher resolution ($\approx 31 \times 11$ arcsec²) than the previously available single dish radio observations. These show a double ring/shell structure for G2.4+1.4, which correlates well with the H α emission, but with no significant linear polarization, which might be expected if the radio emission was non-thermal. [Green & Downes](#) also questioned the non-thermal spectrum reported by [Johnson \(1975\)](#), and hence the SNR identification for G2.4+1.4. The higher frequency flux densities reported by [Johnson \(1975\)](#) are uncertain, and the flux density at 31.4 GHz was based on only a single observation with a 2 arcmin beam, using a 6 arcmin uniform disc model. From the improved resolution available from the VLA image of G2.4+1.4, the position of the single 31.4-GHz observation ($17^{\text{h}}42^{\text{m}}43^{\text{s}}$, $-26^{\circ}10^{\text{m}}4$, B1950.0) lies in a region of low emission, and hence the integrated flux density based on this, and the simple

^{*} email: dag@mrao.cam.ac.uk

¹ In some cases labelled ‘G2.3+1.4’.

Table 1. Radio flux densities for G2.4+1.4 from the literature, and from S-PASS (see Appendix A).

frequency /MHz	resolution /arcmin	flux density		telescope, notes	Reference(s)
		value /Jy	error /Jy		
1410	14	5		Parkes 64 m	Johnson (1975), from Sinclair & Kerr (1971)
2650	7.4	4		Parkes 64 m	Johnson (1975), from Beard et al. (1969)
2695	11.3	2	0.6	NRAO 140 ft	Johnson (1975), from Altenhoff et al. (1970)
5000	3.95	3.0	0.6	Parkes 64 m	Johnson (1975), from Goss & Shaver (1968)
15500	2.2	0.44		Haystack 36.5 m	Johnson (1975)
31400	3.75	0.32	0.26	NRAO 11 m	Johnson (1975)
5000	4	2.5		Parkes 64 m	Caswell & Haynes (1987)
843	1.1	2.61	0.20	Molonglo, total flux density	Gray (1994)
843	1.1	2.55	0.22	Molonglo, excluding SW component	Gray (1994)
1408	9.4	3.46	0.35	Effelsberg 100 m	Gray (1994), from Reich, Reich & Fürst (1990)
2695	4.3	2.20	0.44	Effelsberg 100 m	Gray (1994), from Reich et al. (1984)
1490	0.3	2.4	0.2	VLA	Goss & Lozinskaya (1995)
4850	4.2	3.55		PMN survey, Parkes 64 m	Kuchar & Clark (1997)
8350	9.7	2.58	0.19	GBES 13.7 m	Langston et al. (2000)
605	0.25	2.60	0.26	uGMRT (band 4)	Prajapati et al. (2019)
640	0.25	2.54	0.25	uGMRT (band 4)	Prajapati et al. (2019)
675	0.25	2.23	0.22	uGMRT (band 4)	Prajapati et al. (2019)
710	0.25	2.17	0.22	uGMRT (band 4)	Prajapati et al. (2019)
745	0.25	1.99	0.20	uGMRT (band 4)	Prajapati et al. (2019)
1297	0.25	1.34	0.14	uGMRT (band 5)	Prajapati et al. (2019)
1327	0.25	1.31	0.13	uGMRT (band 5)	Prajapati et al. (2019)
1361	0.25	1.30	0.13	uGMRT (band 5)	Prajapati et al. (2019)
1395	0.25	1.26	0.13	uGMRT (band 5)	Prajapati et al. (2019)
1429	0.25	1.21	0.12	uGMRT (band 5)	Prajapati et al. (2019)
2303	8.9	3.29	0.49	S-PASS, Parkes 64 m	this paper, from Carretti et al. (2019)

uniform disc model – which is smaller than the extent of G2.4+1.4 – will underestimate the true flux density. Furthermore, the limited area observed by Johnson (1975) at 15.5 GHz may not be sufficient to properly define the local background emission away from G2.4+1.4, which would mean the integrated flux density would be an underestimate.

Gray (1994) presented observations of G2.4+1.4 at 843 MHz, and derived a spectral index $\alpha = 0.13^{+0.26}_{-0.23}$ between 843 and 2695 MHz (here α is defined such that flux density S scales with frequency ν as $S \propto \nu^{-\alpha}$), which did not support a non-thermal radio spectrum for G2.4+1.4. The spectral index derived by Gray was based on the integrated 843 MHz flux density, and results from more recent single dish surveys than those available to Johnson (see Section 3 for some further discussion). Goss & Lozinskaya (1995) presented further VLA observations of G2.4+1.4. These, at 1490 MHz, image the extended emission better than the previous VLA observations at 4869 MHz by Green & Downes. Goss & Lozinskaya also conclude that G2.4+1.4 has a flat, thermal radio spectrum. Recently, however, Prajapati et al. (2019) have presented uGMRT observations of G2.4+1.4 in ‘Band 4’ (550–850 MHz) and Band 5 (1050–1450 MHz). From these they derive a non-thermal spectral index of $\alpha = 0.83 \pm 0.10$, quite different from the approximately flat, thermal spectra obtained by Gray (1994) and by Goss & Lozinskaya (1995).

3 THE RADIO SPECTRUM OF G2.4+1.4

Various radio flux densities for G2.4+1.4 from the literature cited in Section 2, and other sources, are given in Table 1 and plotted in Fig. 1. (The resolution of the observations are also listed in Table 1. For the Molonglo and VLA observations, at 843 and 1490 MHz respectively, the geometrical mean of the major and minor axes of the elliptical beam of the observations is given.) These flux densities include a value at 2303 MHz derived from the S-PASS image, see Appendix A.

At 843 MHz, two values are given from Gray (1994), one for the whole source, and the other excluding some emission to southwest which was not seen at 4860 MHz in Green & Downes (1987). The emission in the southwest, with ≈ 60 mJy, was thought probably to be due to an unrelated source with a steep spectrum.

G2.4+1.4 is included in the ‘Tropical’ part of the Parkes–MIT–NRAO (PMN) Survey at 4850 MHz, using observations made with the Parkes 64-m telescope (Griffith et al. 1994). The processing of the PMN observations included the removal of a baseline, using a median filter corresponding to a scale of 57 arcmin, which is several larger than angular extent of G2.4+1.4. In the PMN catalogue the source has a flux density of 1.027 ± 0.054 Jy, from a ‘fixed width’ fit (see Griffith & Wright 1993), including a flag indicating the sources is ‘probably extended’. Given the resolution of the PMN survey is ≈ 4.2 arcmin then G2.4+1.4 is indeed expected to be resolved, so an integrated flux density taking into account its extent is needed. Kuchar & Clark (1997) used the PMN survey images to obtain a peak flux density of 1.025 Jy and angular size of 9.3 arcmin (based on a Gaussian fit) for G2.4+1.4 from the PMN observations. This corresponds to

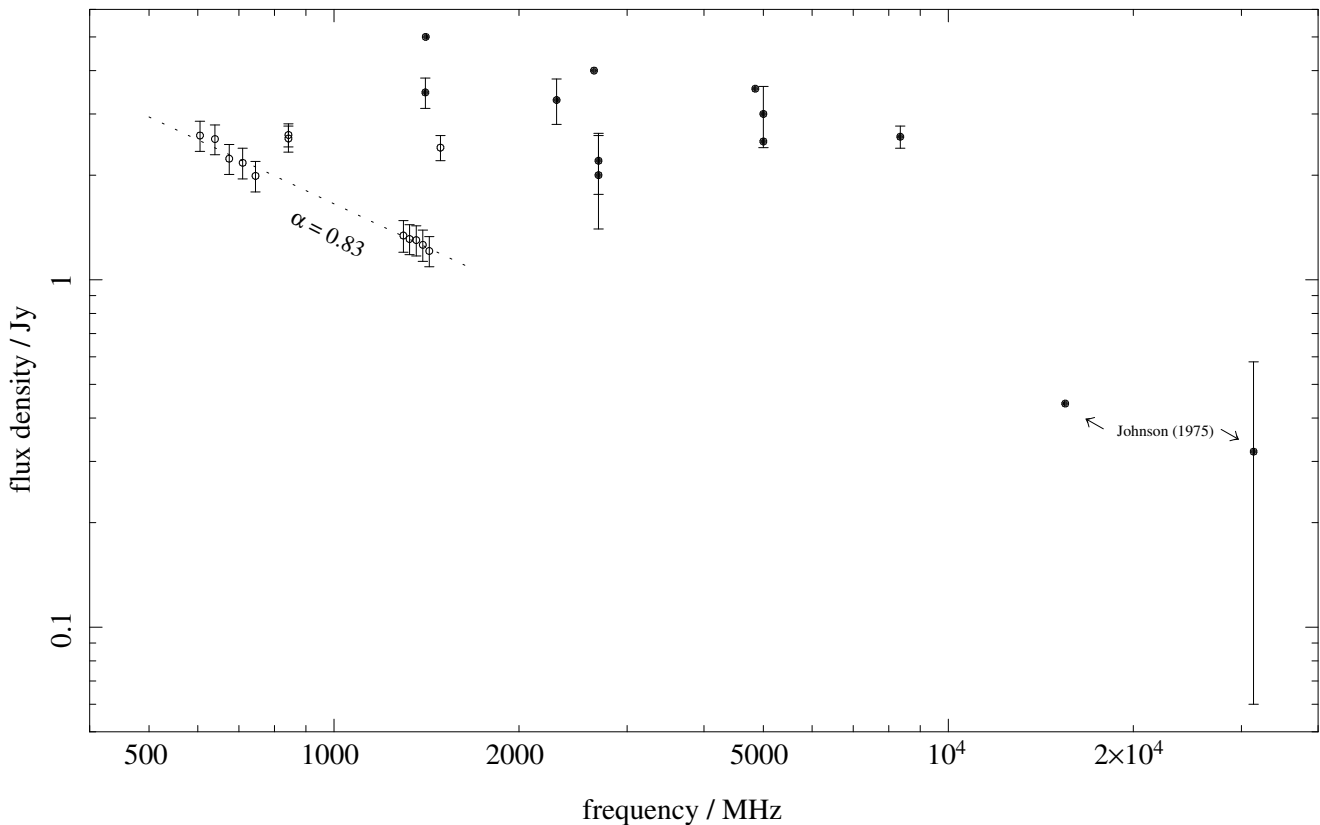


Figure 1. Radio spectrum of G2.4+1.4 using flux densities from the literature, see Table 1. Filled circles are used for flux densities from single dish observations, and open circles are used for flux densities from interferometers, i.e. Molonglo at 843 MHz (Gray 1994), VLA at 1490 MHz (Goss & Lozinskaya 1995), and uGMRT at 605 to 745 MHz and 1297 to 1429 MHz (Prajapati et al. 2019). Error bars are included when flux density errors are available in Table 1. The dotted line shows a non-thermal spectrum with $\alpha = 0.83$ that Prajapati et al. (2019) obtained from their uGMRT flux densities.

an integrated flux density of 3.55 Jy using the formula provided² in Kuchar & Clark (1997). This integrated flux density from Kuchar & Clark (1997) is given in Table 1 and plotted in Fig. 1 rather than the flux density from the PNM catalogue.

In addition G2.4+1.4 is included in the region covered by the GPA survey (Langston et al. 2000), which is at both 8.35 and 14.35 GHz. It is in the source catalogue from this survey, but only at 8.35 GHz, as ‘GPA G002.36+1.42’ (the flux density limits for the two GPA frequencies are 0.9 Jy at 8.35-GHz and 2.5 Jy at 14.35 GHz). This has a peak flux density of 1.65 Jy, and an integrated flux density of 2.58 Jy, with a size of 9.0×5.2 arcmin². The nominal uncertainty in integrated flux density – from both the accuracy of the flux density scale (5.6 per cent) and the rms noise on the images (0.13 Jy beam⁻¹) added in quadrature – is 0.19 Jy.

4 DISCUSSION AND CONCLUSIONS

Comparison of the different flux densities in Table 1 is not straightforward, given G2.4+1.4 is resolved, and the reported flux densities have been integrated in different ways. For example, consider the two flux densities from the Effelsberg 100-m surveys at 1408

and 2695 MHz of $3.46(\pm 10$ per cent) and $2.20(\pm 20$ per cent) Jy respectively, as listed by Gray (1994). These flux densities and errors give a spectral index of $\alpha = 0.70$, but with a large error of ± 0.34 . However, in the Effelsberg 100-m survey catalogues the sizes of the G2.4+1.4 is given as 14.3×14.0 arcmin² at 1408 MHz and 10.8×8.2 arcmin² at 2695 MHz. These sizes correspond to deconvolved sizes 10.8×10.4 arcmin² and 9.9×7.0 arcmin², with the latter being 30 per cent smaller in area, which implies these integrated flux densities are not directly comparable. Another issue is that observations made with interferometers may not recover the total emission from an extended source. If the observations lack sufficiently small baselines to adequately measure the largest scales of the emission from a source, the flux densities will be underestimated. In this case it would be expected that, for a particular set of baselines, this would be more significant at the higher frequencies for observations made over a range of frequencies (as a fixed baseline corresponds to a smaller angular scale at the higher frequencies). This issue potentially applies to several flux densities listed in Table 1: the 843 MHz Molonglo flux densities from Gray (1994); the 1490 MHz VLA flux density from Goss & Lozinskaya (1995); the 605 to 1429 MHz uGMRT flux densities from Prajapati et al. (2019).

If the higher frequency flux densities at 15.5 and 31.4 GHz from Johnson (1975) are discounted – see Section 2 – the available flux densities in Table 1 (see Fig. 1), apart from those from Prajapati et al. are consistent with a flat radio spectrum for G2.4+1.4. A weighted least-square fit to these flux densities which have errors (i.e. those at 843 (the higher, total value), 1408, 1490, 2303, 2695 (two values),

² The integrated flux density is $S_p(\theta/\theta_{\text{psf}})^2$, where S_p is the peak flux density, θ is the fitted angular size, and θ_{psf} is the FWHM of the PMN images, 5 arcmin.

5000 and 8350 MHz in Table 1) gives a spectral index $\alpha = 0.02 \pm 0.08$. For this fit the errors in these flux densities were taken as double the values listed in Table 1, to be cautious (given that flux densities have been derived in different ways, as noted above). This flat spectrum is not consistent with the non-thermal spectrum with $\alpha = 0.83 \pm 0.10$ derived by Prajapati et al., as is seen in Fig. 1. The uGMRT Band 5 flux densities (i.e. 1297 to 1429 MHz) are significantly lower than the integrated flux densities from the Molonglo observations at 843 MHz and the several single dish surveys at ≈ 1.4 to 8.35 GHz. This discrepancy is larger at the higher frequencies within the uGMRT band.

The images shown by Prajapati et al. do not show as much extended emission as is seen in the VLA image by Goss & Lozinskaya (1995). The VLA observations were made in D-configuration, which has better smaller baseline coverage than the uGMRT. This implies that the uGMRT images are missing larger scale emission, and hence will underestimate the flux density of G2.4+1.4. Moreover, the uGMRT images show less extended emission at the higher frequencies. Prajapati et al. used a fixed radius range in the uv -plane, which might be expected to eliminate any problem with missing large scale structure varying with frequency. However, the minimum radius used by Prajapati et al. was small, corresponding to only 35 m at 1429 MHz. The uGMRT does not have good coverage in the uv -plane at this radius (the smallest separations between antennas is ≈ 103 m). Also, at the higher uGMRT frequencies, this minimum uv -radius is less than the 45 m diameter of the uGMRT antennas, so observations from such small baselines will suffer from shadowing between antennas. Moreover, Prajapati et al. calculate their integrated flux densities only for emission greater than a 3σ level, which produces biased results that depend systematically on the σ value.

Given the flux densities for G2.4+1.4 that are available from various surveys, it has a flat, optically thin thermal radio spectrum at gigahertz frequencies. The steep, non-thermal integrated radio spectrum reported by Prajapati et al. (2019) for G2.4+1.4 is not consistent with the flat spectrum from other available observations.

Problems deriving accurate radio spectral indices for extended sources from interferometer observations, which miss large-scale structure, do not appear to be limited to the case of G2.4+1.4. There are several reports, based on VLA observations, of non-thermal radio emission from stellar bow-shocks (Benaglia et al. 2010, 2021; Moutzouri et al. 2022). However, there is extended emission in the region of these sources on scales larger than can be measured by the VLA configuration used (an issue that is worse at the higher frequencies). Hence there are significant systematic uncertainties in the apparent non-thermal spectral indices that have been reported for these sources.

ACKNOWLEDGEMENTS

This research has made use of NASA's Astrophysics Data System, and S-band Polarisation All Sky Survey (S-PASS) data.

DATA AVAILABILITY

The data underlying this article are available in the article, or – for S-PASS – from <https://sites.google.com/inaf.it/spass>.

References

Altenhoff W. J., Downes D., Goad L., Maxwell A., Rinehart R., 1970, *A&AS*, 1, 319

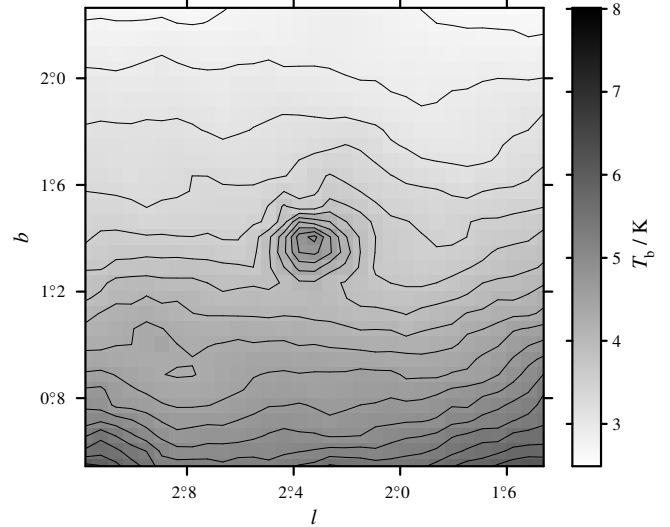


Figure A1. S-PASS image of G2.4+1.4, with Galactic coordinate labels. The contour levels are every 0.2 K in brightness temperature, from 2.7 to 6.1 K, and the greyscale is from 2.0 to 8.0 K.

- Beard M., Thomas B. M., Day G. A., 1969, *Aust. J. Phys. Astrophys. Suppl.*, 11, 27
- Benaglia P., Romero G. E., Martí J., Peri C. S., Araudo A. T., 2010, *A&A*, 517, L10
- Benaglia P., del Palacio S., Hales C., Colazo M. E., 2021, *MNRAS*, 503, 2514
- Carretti E., et al., 2019, *MNRAS*, 489, 2330
- Caswell J. L., Haynes R. F., 1987, *A&A*, 171, 261
- Dopita M. A., Lozinskaya T. A., 1990, *ApJ*, 359, 419
- Dopita M. A., Lozinskaya T. A., McGregor P. J., Rawlings S. J., 1990, *ApJ*, 351, 563
- Goss W. M., Lozinskaya T. A., 1995, *ApJ*, 439, 637
- Goss W. M., Shaver P. A., 1968, *ApJ*, 154, L75
- Gray A. D., 1994, *MNRAS*, 270, 835
- Green D. A., 1984, *MNRAS*, 209, 449
- Green D. A., 1988, *Ap&SS*, 148, 3
- Green D. A., Downes A. J. B., 1987, *MNRAS*, 225, 221
- Griffith M. R., Wright A. E., 1993, *AJ*, 105, 1666
- Griffith M. R., Wright A. E., Burke B. F., Ekers R. D., 1994, *ApJS*, 90, 179
- Johnson H. M., 1975, *ApJ*, 198, 111
- Kuchar T. A., Clark F. O., 1997, *ApJ*, 488, 224
- Langston G., Minter A., D'Addario L., Eberhardt K., Koski K., Zuber J., 2000, *AJ*, 119, 2801
- Meyers B. W., et al., 2017, *Publ. Astron. Soc. Aust.*, 34, e013
- Milne D. K., 1979, *Aust. J. Phys.*, 32, 83
- Moutzouri M., et al., 2022, *A&A*, 633, A80.
- Prajapati P., Tej A., del Palacio S., Benaglia P., CH I.-C., Vig S., Mandal S., Kanti Ghosh S., 2019, *ApJ*, 884, L49
- Reich W., Fürst E., Haslam C. G. T., Steffen P., Reif K., 1984, *A&AS*, 58, 197
- Reich W., Reich P., Fürst E., 1990, *A&AS*, 83, 539
- Sinclair M. W., Kerr F. J., 1971, *Aust. J. Phys.*, 24, 769
- Treffers R. R., Chu Y.-H., 1982, *ApJ*, 254, 132

APPENDIX A: A 2303-MHz FLUX DENSITY FROM S-PASS

G2.4+1.4 is included in the region covered by the S-band Polarisation All Sky Survey (S-PASS), see Carretti et al. (2019). The S-PASS observations were made at 2303 MHz with the Parkes 64-m telescope, with a resolution of 8.9 arcmin. As the source catalogue from S-PASS (Meyers et al. 2017) excludes Galactic latitudes with $|b| < 10^\circ$, an integrated flux density for G2.4+1.4 is derived here from the S-PASS

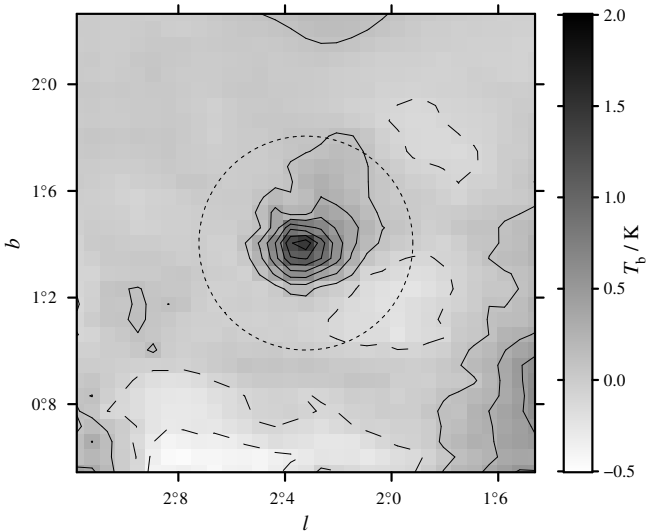


Figure A2. S-PASS image of G2.4+1.4, with Galactic coordinate labels, after latitude dependant background removal (see text). The contours are $\pm 0.3, \pm 0.1, 0.1, 0.3, \dots, 1.3$ K in brightness temperature, with negative contours dashed, and the greyscale is from -0.5 to 2.0 K. The dotted circle indicates the area integrated for the flux density of G2.4+1.4.

image³. Figure A1 shows the S-PASS image of G2.4+1.4 and its surroundings, which clearly shows G2.4+1.4, with a peak of ≈ 5 K. This is ≈ 1.5 K above the local background level, which corresponds to $\approx 1.8 \text{ Jy beam}^{-1}$. However, as G2.4+1.4 is slightly resolved in S-PASS, an integrated flux density is required, which needs to take into account the local background emission (which is at about twice the level of the peak excess seen for G2.4+1.4). In this case the background gradient is larger at lower Galactic latitudes than at higher latitudes. Hence simply averaging the local emission outside G2.4+1.4 in an annulus would provide a biased estimate of local background. However, from Fig. A1 it is evident that the variation in the background emission is largely with Galactic latitude. The background emission at a particular latitude, i.e. each row in Fig. A1, was estimated by taking the median of selected pixel values in the row. The selected pixels excluded the central third of each row, to exclude the emission from G2.4+1.4 (i.e. the regions with Galactic longitude from approximately $1:5$ to $2:0$ and $2:6$ to $3:2$ were used). Figure A2 shows the S-PASS image after removal of this latitude dependant background estimate. The integrated emission from G2.4+1.4 in Fig. A2, within the circle shown, is 3.26 Jy . The radius of the circle is 7 pixels (each 3.44 arcmin), i.e. about 24 arcmin . This radius is the approximate radius of G2.4+1.4 seen in higher resolution images (i.e. $\approx 6 \text{ arcmin}$), plus twice the S-PASS resolution. The integrated flux density derived varies if the background removal uses different ranges of Galactic longitude, or if a different integration radius is chosen. For example, if the integration radius of is changed by 1 pixel then the integrated flux density changes by 4 per cent. To be cautious I assign an considerably larger error of 15 per cent to this integrated flux density (which is larger than the flux density scale uncertainty of 5 per cent for S-PASS), i.e. 0.49 Jy .

This paper has been typeset from a $\text{\TeX}/\text{\LaTeX}$ file prepared by the author.

³ See: <https://sites.google.com/inaf.it/spass>.